DOI: 10.6060/ivkkt.20216411.6478

УДК: 54.057:549.613.4

# ФИЗИКО-ХИМИЧЕСКОЕ ИЗУЧЕНИЕ ПОВЕДЕНИЯ МУЛЛИТОВОГО ПРЕКУРСОРА, СИНТЕЗИРОВАННОГО СООСАЖДЕНИЕМ

**Н.В. Филатова, Н.Ф. Косенко, М.А. Баданов**

Наталья Владимировна Филатова *, Надежда Федоровна Косенко, Максим Анатольевич Баданов

Кафедра технологии керамики и наноматериалов, Ивановский государственный химико-технологический университет, пр. Шереметевский, 7, Иваново, Российская Федерация, 153000
E-mail: zyanata@mail.ru *, nfkosenko@gmail.com, m.badanov90@gmail.com

***Изучено соосаждение аммиаком гидратированных форм оксидов алюминия и кремния. Термограммы высушенного соосажденного продукта показали, что при низких температурах (до ~300 °С) имелся набор слабо выраженных пиков от дегидратации адсорбированной и гидратной воды. Затем наблюдалось плавное удаление воды до ~600 °С, соответствовавшее переходу гидроксид алюминия $Al(OH)_3$ → моногидрат (бёмит) γ-AlOOH. Впоследствии масса пробы оставалась постоянной, поэтому наблюдаемые экзотермические пики могли быть вызваны образованием шпинели (около 900 °С) и кристаллизацией муллита из шпинельной фазы (выше 1200 °С). После прокаливания при 900–1000 °С преобладала алюмосиликатная шпинельная фаза со структурой γ-$Al_2O_3$, хотя проявлялись слабые признаки кристаллического муллита. Высокая дисперсность гидратированных частиц оксидов алюминия и кремния предопределяла их значительную реакционную способность. В результате муллит появлялся при относительно низкой температуре. Острые пики, которые относились к однофазному орторомбическому муллиту, регистрировались, начиная с 1150–1200 °С; в то же время рефлексы шпинели практически исчезали. Наиболее интенсивные фазовые изменения происходили в диапазоне 1100–1200 °С. Положения и интенсивность пиков хорошо согласовывались со справочными данными для муллита. Определены параметры кристаллической решетки этой фазы. Средний размер кристаллитов находился в пределах от 6,3 нм при 1100 °С до 7,4 нм при 1200 °С. Рассчитанное неизотермическим методом (по уравнению Аврами) значение эффективной энергии активации кристаллизации муллита составило (740 ± 40) кДж/моль, что хорошо согласуется с энергией активации диффузии ионов $Si^{4+}$ в слое муллита (от 730 до 780 кДж/моль по литературным данным). Можно предположить, что процесс лимитировался диффузией ионов $Si^{4+}$.***

**Ключевые слова:** муллит, синтез соосаждением, гетерогенное соосаждение, кинетика кристаллизации, уравнение Аврами, энергия активации

# PHYSICO-CHEMICAL STUDY OF THE BEHAVIOR OF A MULLITE PRECURSOR SYNTHESIZED WITH CO-PRECIPITATION

**N.V. Filatova, N.F. Kosenko, M.A. Badanov**

Natalya V. Filatova*, Nadezhda F. Kosenko, Maxim A. Badanov

Department of Technology of Ceramics and Nanomaterials, Ivanovo State University of Chemistry and Technology, Sheremetevskiy ave., 7, Ivanovo, 153000, Russia
E-mail: zyanata@mail.ru*, nfkosenko@gmail.com, m.badanov90@gmail.com

***The co-precipitation of hydrated forms of aluminum oxide and silica with the addition of ammonia has been studied. Thermal curves of a dried co-precipitated product showed that at low temperature (up to ~300 °C) there was a set of clearly defined endothermic peaks which resulted from dehydration of adsorbed and hydrated water. Then, a gradual removal of water was observed up to ~ 600 °C, which corresponded to the transition aluminum hydroxide $Al(OH)_3$ → monohydrate***

***(boehmite) γ-AlOOH. After it, the sample weight remained constant, and exothermic peaks were because of the spinel formation (about 900 °C) and the mullite crystallization from the spinel phase (above 1200 °C). After calcination at 900–1000 °C, the Al–Si spinel phase of γ-$Al_2O_3$ type was dominated, though some slight signs of crystalline mullite were already appeared. The high dispersion of hydrated alumina and silica particles determined their considerable reactivity. It resulted in the mullite appearance at a rather low temperature. Sharp peaks which concerned to single orthorhombic mullite were registered since 1150–1200 °C. At the same time, the spinel reflexes practically disappeared. The most intensive phase changes were in the range of 1100–1200 °C. The peak positions and intensity of calcined products agreed well with the reference data for mullite. Its lattice parameters were determined. The average crystallite size was ranged from 6.3 nm at 1100 °C to 7.4 nm at 1200 °C. The effective activation energy was calculated by non-isothermal method (Avrami equation) as (740 ± 40) kJ/mol. This magnitude was in a well accordance with the activation energy values for the diffusion of the $Si^{4+}$ ions in the mullite layer which were estimated to range from 730 to 780 kJ/mol (literature data). So, one might assume that the limiting stage was just the diffusion of the $Si^{4+}$ ions.***

**Key words:** mullite, co-precipitation synthesis, heterogeneous co-precipitation, crystallization kinetics, Avrami equation, activation energy

**Для цитирования:**
Филатова Н.В., Косенко Н.Ф., Баданов М.А. Физико-химическое изучение поведения муллитового прекурсора, синтезированного соосаждением. *Изв. вузов. Химия и хим. технология*. 2021. Т. 64. Вып. 11. С. 97–102

**For citation:**
Filatova N.V., Kosenko N.F., Badanov M.A. Physico-chemical study of the behavior of a mullite precursor synthesized with co-precipitation. *ChemChemTech* [*Izv. Vyssh. Uchebn. Zaved. Khim. Khim. Tekhnol*.]. 2021. V. 64. N 11. P. 97–102

## INTRODUCTION

Mullite $3Al_2O_3{\cdot}2SiO_2$ is the only compound in the system $Al_2O_3$ – $SiO_2$ which exists at atmospheric pressure. It has unique physical and chemical properties and technological possibilities such as high melting point, excellent high temperature mechanical properties, good chemical and thermal stability, high creep resistance, high corrosion resistance even in harsh environments, low thermal expansion associated with excellent thermal shock resistance, and low thermal and electrical conductivity, dielectric properties, etc. [1-9]. So, mullite is among the most studied binary oxides.

Mullite is synthesized by means of different ways, namely: solid-phase reaction [10, 11], arc plasma melting [12], spark plasma sintering [13], microwave-assisted synthesis [14], mechanochemistry-aided [15], spray pyrolysis [16], molten media [17], etc.

During recent years, a considerable quantity of studies was devoted to the obtaining of precursors, simplifying the following mullite synthesis. Among them it should be noted works on nucleation and growth processing using various suspensions such as sol-gel systems [18, 19], coprecipitated dispersions [20, 21]. These methods allow to obtain fine precipitates which can sinter at lower temperatures. At the same time, it is achieved a high homogeneity and a heightened purity ensuring improved and reproducible properties of ceramic materials at decreased temperatures. Kinetics and mechanism of the mullite formation and crystallization are also under consideration [22-29].

The present study mainly concerns the behavior of mullite precursor synthesized by coprecipitation with ammonia. There was also tried to value an activation energy for mullite crystallization from obtained diphasic suspension.

## MATERIALS AND EXPERIMENTS

Sodium metasilicate pentahydrate $Na_2SiO_3{\cdot}5H_2O$, analytical grade, had the common alkalinity in terms of $Na_2O$ 28-30; module $SiO_2/Na_2O$ 0.9-1.0; iron in terms of $Fe_2O_3$ no more than 0.02%; insoluble in water impurities 0,01-0,06; water no more than 45.

Aluminum nitrate nonahydrate $Al(NO_3)_3{\cdot}9H_2O$, analytically grade, in the form of 0.25 M solution in a distilled water and aqueous colloidal silica, derived from sodium metasilicate pentahydrate by an ion exchange method, were mixed together under stirring. The relative amounts of $Al_2O_3$ and $SiO_2$ were chosen to be equal to the composition of mullite $3Al_2O_3{\cdot}2SiO_2$. The ammonium hydroxide solution (chemically pure, 6 M) was added to a mixed solution under constant stirring to pH 6.5-7. The precipitate was filtered, washed with distilled water, filtered again, and dried at 100-105 °C to a powder which was ground in a mortar.

Dried precursors were heated (calcined) at a rate of 10 °C/min in air atmosphere up to required temperature in a muffle oven SNOL 1300/1600.

XRD-patterns were obtained using a diffractometer DRON-6 with a copper target (λ = 1.54 Å), a graphite diffracted beam monochromator, and a working voltage and current of 40 kV and 100 mA, respectively. XRD peaks for 2θ 16.48, 26.31, 31.10, 33.31, 35.39, 37.14, 39.38, 41.01, 42.73 corresponded to orthorhombic lattice planes of mullite (110), (210), (001), (220), (111), (130), (201), (121), (230), respectively (BRUFF ID R141103.9). The quantitative XRD analysis was made analyzing mullite reflexes using calcium fluoride as an internal standard.

Differential thermal analysis (DTA/DSC) and thermogravimetric analysis (TGA) were performed in a computer-controlled instrument (model TGA/SDTA851$^e$/LF/1600); crucible 700 mkL; air blow 50 mL/min; temperature program up to 1400 °C at various heating rates (1, 3, 5, 10, 15, 20, 30, and 50 °C/min).

## RESULTS AND DISCUSSION

During ammonia addition there was the coprecipitation of hydrated forms of alumina and silica. Even after drying the precipitate kept a considerable quantity of water. Figure 1 shows DSC and TG curves of a dried coprecipitated product. At low temperature (up to ~300 °C) there was a set of clearly defined endothermic peaks which resulted from dehydration of adsorbed and hydrated water. Then a slow water removal up to ~600 °C corresponded to alumina trihydrate $Al(OH)_3$ → monohydrate (boehmite) AlOOH transformation. After it, the sample weight remained constant, and exothermic peaks were because of the spinel formation (about 900 °C) and the mullite crystallization from the spinel phase (above 1200 °C).

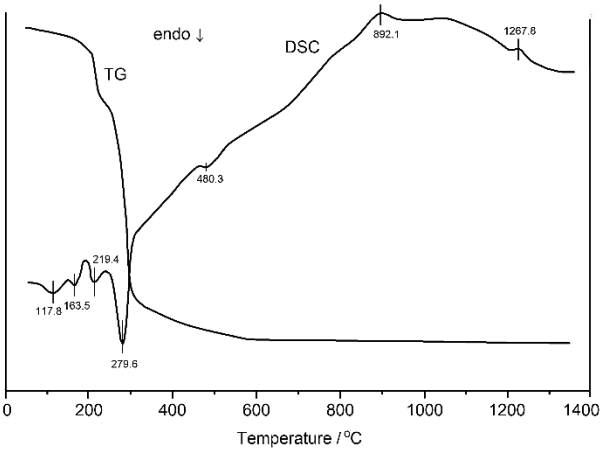


Fig. 1. TG-DSC curves of a dried co-precipitated product
Рис. 1. Кривые ТГ и ДСК для высушенного соосажденного продукта

Fig. 2 shows the X-ray diffraction analysis (XRD) patterns of the mullite precursors calcined from 800 to 1200 °C for 2 h. The results of the XRD indicated that before 800 °C there were only amorphous phases. The wide amorphous band at 2θ = 20-22° may be related to amorphous silica.

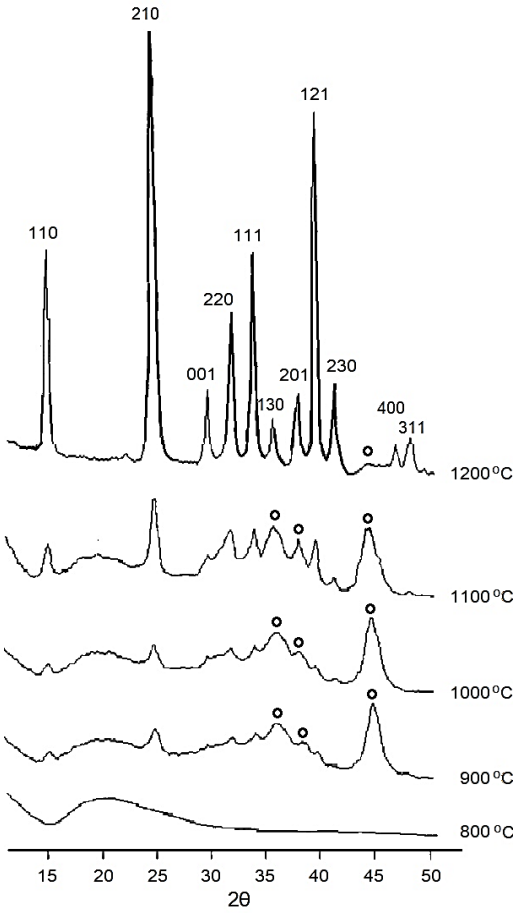


Fig. 2. XRD patterns of mullite precursors calcined at various temperatures. Marks o denote spinel phase of γ-$Al_2O_3$ type. The rest refers to mullite
Рис. 2. Дифрактограммы прекурсоров муллита, прокаленных при различных температурах. Значки о означают шпинельную фазу типа γ-$Al_2O_3$. Остальные пики относятся к муллиту

After calcination at 900-1000 °C, the Al–Si spinel phase of γ-$Al_2O_3$ type was dominated, though some slight signs of crystalline mullite were already appeared. The high dispersion of hydrated alumina and silica particles determined their considerable reactivity. It resulted in the mullite appearance at a rather low temperature. Sharp peaks which concerned to single orthorhombic mullite were registered since 1150-1200 °C; at the same time, the spinel reflexes practically disappeared. The most intensive phase changes were in the range of 1100-1200 °C (Fig. 2, Table 1). The peak positions and intensity of calcined products agreed well with the reference data for mullite.

***Table 1***

**The phase changes in the co-precipitated mullite precursor composition**

***Таблица 1.*** **Фазовые изменения состава соосажденного прекурсора муллита**

| Temperature, °C | Phase content, % | | |
|---|---|---|---|
| | X-ray amorphous | Spinel of γ-$Al_2O_3$ type | Mullite |
| 800 | 100 | 0 | 0 |
| 900 | 45 | 47 | 8 |
| 1000 | 33 | 56 | 11 |
| 1100 | 14 | 59 | 28 |
| 1200 | 2 | 3 | 95 |
| 1300 | 0 | 0 | 99 |
| 1400 | 0 | 0 | 100 |

X-ray amorphous phase can represent amorphous substances or crystals with very small dimensions of coherent-scattering region and/or having a lot of defects. Its quantity $m_{am}$ was calculated by equation:

$$m_{am} = 100 - \Sigma m_{cr}, \quad (1)$$

where $\Sigma m_{cr}$ – total content of crystalline phases.

The lattice parameters of this phase were determined to be $a$ = 0.7553 nm, $b$ = 0.7668 nm, and $c$ = 0.2881 nm, agreeing with the data of stoichiometric mullite (BRUFF ID R141103.9): $a$ = 0.75520 nm, $b$ = 0.76660 nm, and $c$ = 0.28760 nm.

The crystallite size $D$ of powders was estimated according to the Debay-Scherrer equation:

$$D = 0.90\lambda/\beta \cos\theta, \quad (2)$$

where λ – X-ray wavelength; β and θ – full-width-at-half-maximum (FWHM) of an observed peak and diffraction angle, respectively.

The calculation of the average crystallite size was made using the strongest mullite reflexes. The results showed that $D$ value was ranged from 6.3 nm at 1100 °C to 7.4 nm at 1200 °C.

In the paper [30] there was analyzed the mullite formation kinetics from precursors obtained by means of sol-gel method. Reaction kinetics in diphasic and monophasic gels was compared. It was ascertained that the mullite formation in diphasic gels could be described by the Avrami equation, which was characteristic of the crystal growth mechanism controlled by the diffusion. This process started at ~1250 °C and had the activation energy about $10^3$ kJ/mol. As under coprecipitation we obtained a microheterogeneous suspension, i.e. diphasic system, it attempted to get the activation energy $E_a$ according to the Avrami equation:

$$ln\left(\frac{T_{max}^2}{h}\right) = \frac{E_a}{RT_{max}} + ln\frac{E_a}{RA}, \quad (3)$$

where $T_{max}$ – temperature of the exothermic peak which related to the mullite formation on the DSC curve, $h$ – heating rate, *K/sec*, $R$ – universal gas constant (8.314 J/mol·K); $A$ – preexponential factor of the Arrhenius equation:

$$k = A \exp(-E_a/RT), \quad (4)$$

where k – a reaction rate constant.

According to the equation (4) the activation energy $E_a$ can be determined by the slope ratio tgα of the $ln\left(\frac{T_{max}^2}{h}\right) - \frac{1}{T_{max}}$ graph. $E_a = R \cdot tg\alpha$.

Examples of DSC curve fragments for some mullite forming suspensions synthesized at pH 6.5 are given in Fig. 3.

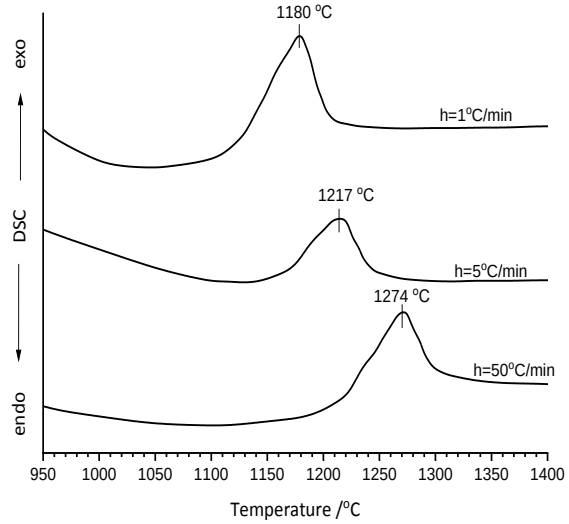


Fig. 3. DSC curve fragments for some mullite forming suspensions synthesized at pH 6.5 at various heating rates of samples

Рис. 3. Фрагменты кривых ДТА для МОС, синтезированных при pH 6,5, при различной скорости нагревания образцов

The crystallization of amorphous substances is always accompanied by the heat release that is expressed as exothermal effect on the DTA/DSC curve. Under heating rate increase the DTA/DSC curve deviation which was related to a phase transformation was shifted to the higher temperatures. Fragments which are shown on Fig. 3 differ by the heating rate during dependence registration.

Experimental and calculated data are given in Table 2.

***Table 2***

**Data for the activation energy determination by the Avrami equation**

**Таблица 2. Данные для определения энергии активации по уравнению Аврами**

| $T_{max}$, °C | T, K | h, K/min |
|---|---|---|
| 1180 | 1453 | 1 |
| 1203 | 1476 | 3 |
| 1217 | 1490 | 5 |
| 1223 | 1496 | 10 |
| 1242 | 1515 | 15 |
| 1252 | 1525 | 20 |
| 1260 | 1533 | 30 |
| 1274 | 1547 | 50 |

The Avrami plot of the mullite crystallization from coprecipitated mullite precursors is shown on Fig. 4.

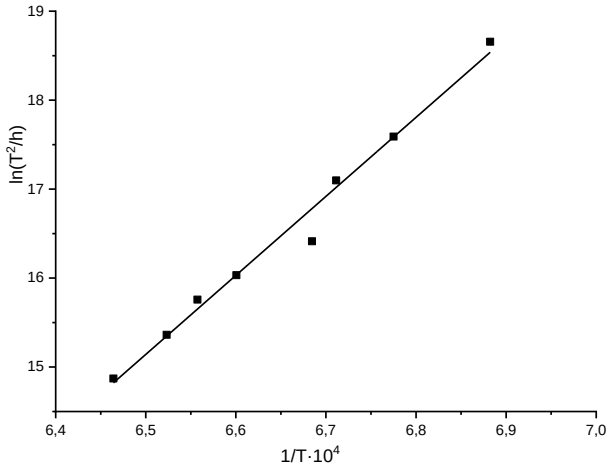


Fig. 4. The Avrami plot of the mullite crystallization from co-precipitated mullite precursors at pH 6.5

Рис. 4. Зависимость в координатах уравнения Аврами для процесса кристаллизации муллита из соосажденных прекурсоров муллита

The slope ratio tgα was equal to 89.0 ± 4.6. Therefore, the calculated value of the effective activation energy was (740 ± 40) kJ/mol. This magnitude was in a well accordance with the activation energy values for the diffusion of the $Si^{4+}$ ions in the mullite layer which were estimated to range from 730 to 780 kJ/mol [22]. So, one might assume that the limiting stage was just the diffusion of the $Si^{4+}$ ions.

## CONCLUSION

A mullite precursor in the form of a microheterogeneous suspension was synthesized by coprecipitation with ammonia from an aluminum nitrate solution and colloidal silica. The obtained suspensions had a higher reactivity because of the considerable dispersion and an amorphous structure. The chemically precipitated mullite precursor transformed easily into mullite during a heat treatment. It was suggested the following sequence of the mullite formation from a coprecipitated by ammonia precursor at pH 6.5: amorphous phase $\frac{900\,^{\circ}C}{2\,h}\rightarrow$ Al-Si spinel of γ-$Al_2O_3$ type $\frac{1100-1200\,^{\circ}C}{2\,h}\rightarrow$ crystallized mullite. The final product was the stoichiometric orthorhombic mullite with parameters corresponding to reference data. The results obtained by means of the X-ray diffraction method and the thermal analysis are in accordance together.

The effective activation energy of the mullite crystallization from a mullite forming suspension was calculated by the Avrami equation. Its value was (740 ± 40) kJ/mol that corresponded to the activation energy values for the diffusion of the $Si^{4+}$ ions in the mullite layer ((730–780) kJ/mol) given in a literature.

## ACKNOWLEDGEMENTS

*The study was carried out using the resources of the Center for Shared Use of Scientific Equipment of the ISUCT (with the support of the Ministry of Science and Higher Education of Russia, grant No. 075-15-2021-671).*

*The authors declare the absence a conflict of interest warranting disclosure in this article.*

*Исследование проведено с использованием ресурсов Центра коллективного пользования научным оборудованием ИГХТУ (при поддержке Минобрнауки России, соглашение № 075-15-2021-671).*

*Авторы заявляют об отсутствии конфликта интересов, требующего раскрытия в данной статье.*

## REFERENCES
## ЛИТЕРАТУРА

1. **Schneider H., Komarneni S.** Mullite. John Wiley & Sons. Weinheim. Germany. 2006. 509 p. DOI: 10.1002/3527607358.
2. **Schneider H., Schreuer J., Hildmann B.** Structure and properties of mullite – A review. *J. Eur. Ceram. Soc.* 2008. V. 28. N 2. P. 329–344. DOI: 10.1016/j.jeurceramsoc.2007.03.017.
3. **Duval D.J., Risbud S.H., Shackelford J.F.** Mullite, in: Ceramic and Glass Material. Springer. 2008. P. 27–39. DOI: 10.1007/978-0-387-73362-3_2.
4. **Aryal S., Rulis P., Ching W.** Mechanical properties and electronic structure of mullite phases using first-principles modeling. *J. Am. Ceram. Soc.* 2012. V. 95. N 7. P. 2075–2088. DOI: 10.1111/j.1551-2916.2012.05172.x.
5. **Malki M., Hoo Ch.M., Mecartney M. L., Schneider H., Wei W.-C. J.** Electrical Conductivity of Mullite Ceramics. *J. Amer. Cer. Soc.* 2014. V. 97. N 6. P. 1923-1930. DOI: 10.1111/jace.12867.
6. **Zhang Ch., Jiang Y., Ma Y.** Optical floating zone growth and dielectric constants of near-3:2mullite crystals. *J. Eur. Cer. Soc.* 2016. V. 36. N 3. P. 577–581. DOI: 10.1016/j.jeurceramsoc.2015.10.025.
7. **Hirata Y., Shimonosono T., Itoh Sh., Kiritoshi Sh.** Theoretical and experimental analyses of thermal properties of dense polycrystalline mullite. *Ceramics Int.* 2017. V. 43. N 13. P. 10410–10414. DOI: 10.1016/j.ceramint.2017.05.076.
8. **Murshed M.M., Šehović M., Fischer M., Senyshyn A., Schneider H., Gesing Th.M.** Thermal behavior of mullite between 4 K and 1320 K. *J. Amer. Cer. Soc.* 2017. V. 100. N 11. P. 5259-5273. DOI: 10.1111/jace.15028.
9. **Krenzel Th.F., Schreuer J., Laubner D., Cichocki M., Schneider H.** Thermo-mechanical properties of mullite ceramics: New data. *J. Amer. Cer. Soc.* 2019. V. 102. N 1. P. 416–426. DOI: 10.1111/jace.15925.
10. **Yu P.-Ch., Tsai Y.-W., Yen F.-S., Yang W.-P., Huang Ch.-Liang.** Thermal characteristic difference between α-$Al_2O_3$ and cristobalite powders during mullite synthesis induced by size reduction. *J. Eur. Cer. Soc.* 2015. V. 35. N 2. P. 673-680. DOI: 10.1016/j.jeurceramsoc.2014.08.040.

11. **Vargas F., Restrepo E., Rodríguez J.E., Vargas F., Arbeláez L., Caballero P., Arias J., López E., Latorre G., Duarte G.** Solid-state synthesis of mullite from spent catalysts for manufacturing refractory brick coatings. *Cer. Int.* 2017. V. 44. N 4. P. 3556. DOI: 10.1016/j.ceramint.2017.11.044.
12. **Yugeswaran S. Suresh K. Selvarajan V. Lusvarghi L. Karoly Z. Szépvölgyi J.** Synthesis of mullite by means of transferred and nontransferred arc plasma melting. *Mater. Manuf. Proc.* 2010. V. 25. N 9. P. 909. DOI: 10.1080/10426910903536725.
13. **Zhang J., Zhan H., Fu Zh., Todd R.I.** In-situ synthesis and sintering of mullite glass composites by SPS. *J. Adv. Cer.* 2014. V. 3. N 2. P. 165. DOI: 10.1007/s40145-014-0108-y.
14. **Ebadzadeh T., Sarrafi M.H., Salahi E.** Microwave-assisted synthesis and sintering of mullite. *Cer. Int.* 2009. V. 35. N 8. P. 3175-3179. DOI: 10.1016/j.ceramint.2009.05.013.
15. **Mizuno M., Saito H.** Preparation of highly pure fine mullite powder. *J. Amer. Cer. Soc.* 2005. V. 72. N 3. P. 377-382. DOI: 10.1111/j.1151-2916.1989.tb06139.x.
16. **Sanz J., Sobrados I., Cavalieri A.L., Pena P., Aza S. Moya J.S.** Structural changes induced on mullite precursors by thermal treatment: A 27Al MAS-NMR Investigation. *J. Amer. Cer. Soc.* 1991. V. 74. N 10. P. 2398-2403. DOI: 10.1111/j.1151-2916.1991.tb06775.x.
17. **Zhu B.Q., Li X.D., Hao R., Wang H.** Preparation of mullite powder by aluminum sulfate and silica in molten sodium sulfate. *Key Eng. Mater.* 2007. V. 336-338. P. 924-926. DOI: 10.4028/www.scientific.net/KEM.336-338.924.
18. **Rajaei H., Mobasherpour I., Farvizi M., Zakeri M.** Effect of mullite synthesis methods on the spark plasma sintering behaviour and mechanical properties. *Micro Nano Lett.* 2016. V. 11. N 8. P. 465-468. DOI: 10.1049/mnl.2016.0092.
19. **Buljan I., Kosanović C., Kralj D.** A novel synthesis of nanosized mullite from aluminosilicate precursors. *J. All. Comps.* 2011. V. 509. N 32. P. 8256-8261. DOI: 10.1016/j.jallcom.2011.05.099.
20. **Aschauer U., Burgos-Montes O., Moreno R., Bowen P.** Hamaker 2: A toolkit for the calculation of particle interactions and suspension stability and its application to mullite synthesis by colloidal methods. *J. Disp. Sci. Technol.* 2011 V. 32. N 4. P. 470-479. DOI: 10.1080/01932691003756738.
21. **Sanad M.M.S., Rashad M.M., Abdel-Aal E.A., El-Shahat M.F.** Synthesis and characterization of nanocrystalline mullite powders at low annealing temperature using a new technique. *J. Eur. Cer. Soc.* 2012. V. 32. N 16. P. 4249-4255. DOI: 10.1016/j.jeurceramsoc.2012.07.014.
22. **Sung Y.-M.** Kinetics analysis of mullite formation reaction at high temperatures. *Acta Mater.* 2000. V. 4. N 9. P. 2157-2162. DOI: 10.1016/S1359-6454(00)00032-X.
23. **Francis A., Vilminot S.** Crystallisation kinetics of mullite glass-ceramics obtained from alumina–silica wastes. *Int. J. Sustainable Eng.* 2012. V. 6. N 1. P. 74-81. DOI: 10.1080/19397038.2012.672478.
24. **Griggio F., Bernardo E., Colombo P., Messing G.L.** Kinetic studies of mullite synthesis from alumina nanoparticles and a preceramic polymer. *J. Amer. Cer. Soc.* 2008. V. 91. N 8. P. 2529-2533. DOI: 10.1111/j.1551-2916.2008.02515.x.
25. **Belhouchet H., Hamidouche M., Torrecillas R., Fantozzi G.** The non-isothermal kinetics of mullite formation in boehmite–zircon mixtures. *J. Therm. Anal. Calor.* 2014. V. 116. N 2. P. 795-803. DOI: 10.1007/s10973-013-3601-6.
26. **Okada K.** Activation energy of mullitization from various starting materials. *J. Eur. Cer. Soc.* 2008. V. 28. N 2. P. 377-382. DOI: 10.1016/j.jeurceramsoc.2007.03.015.
27. **Vieira S.C., Ramos A.S., Vieira M.T.** Mullitization kinetics from silica- and alumina-rich wastes. *Cer. Int.* 2007. V. 33. N 1. P. 59-66. DOI: 10.1016/j.ceramint.2005.07.015.
28. **De Oliveira T.C., Ribeiro C.A., Brunelli D.D., Rodrigues L.A., Thim G.P.** The kinetic of mullite crystallization: effect of water content. *J. Non-Cryst. Solids.* 2010. V. 356. N 52-54. P. 2980-2985. DOI: 10.1016/j.jnoncrysol.2010.05.078.
29. **Magliano M.V.M., Pandolfelli V.C.** Mulitização em refratários utilizando diferentes fontes precursoras: revisão. *Cerâmica*. 2010. N 56. P. 368-375. DOI: 10.1590/S0366-69132010000400009.
30. **Li D.X., Thomson W.J.** Kinetic mechanisms for mullite formation from sol-gel precursors. *J. Mater. Res.* 1990. V. 5. P. 1963–1969. DOI: 10.1557/JMR.1990.1963.


*Поступила в редакцию 07.06.2021*
*Принята к опубликованию 26.07.2021*

*Received 07.06.2021*
*Accepted 26.07.2021*